

Surrogate assisted reliability-based design
optimization of novel Spear-In-Sand launch
vehicle spent stage recovery approach using
Monte Carlo simulations

Deva Karthik Lakshman Dasu^{1*} and Pankaj Priyadarshi ²

¹Aerospace Mechanisms Group, Vikram Sarabhai Space Center, Veli,
Thiruvananthapuram, Kerala, India, 695022.

²Advanced Technology Vehicle Project, Vikram Sarabhai Space Center,
Veli, Thiruvananthapuram, Kerala, India, 695022.

*Corresponding author(s). E-mail(s): karthiklakshmandasu@gmail.com;
Contributing authors: pankaj.priyadarshi@gmail.com;

Note: This article is under internal review and has not yet been peer-reviewed.

1 Introduction

Recovery of the launch vehicle spent stage allows for low-cost and environment-friendly access to space. There are various methods for recovering a spent stage; the Vertical Takeoff Vertical Landing (VTVL) method is one of the proven methods in the current times. The SpaceX Falcon 9 is the first operational launch vehicle to recover the spent stage using the VTVL recovery method. The thrust-to-weight ratio in descent plays a crucial role in the VTVL recovery method. The Falcon 9 uses only one out of nine engines during the descent to attain zero velocity and body rates at touchdown. Furthermore, the thrust from one engine can be throttled down to nearly 57%, which makes the total thrust in final burn nearly 6.3% of the total thrust in ascent ([SpaceX \(2025\)](#)). This thrust reduction is categorized as *deep throttling*, and cause severe combustion instabilities for stages with one or few large engines ([Casiano et al. \(2010\)](#)).

A novel spent-stage recovery method, known as the Spear-In-Sand (SIS) method, is proposed in Vikram Sarabhai Space Center (VSSC) for stages with large engines, which eliminates the need for deep throttling while landing in vertical mode. The proposed method eliminates the need for zero velocity and body rates at touchdown. In this method, the spent stage is attached with sharp spear-shaped landing legs (shown in figure 1a) and is decelerated to the minimum possible velocity and body rates without deep throttling. Furthermore, the attitude of the stage need not be exactly vertical. Instead of landing on a rigid surface, the spent stage is allowed to land on a pre-designed and fully prepared sand bed to reduce the impact. The terminal velocity, attitude, and body rate constitute the state vector of the spent stage during the touchdown. The residual kinetic energy of the stage dissipates in the form of penetration of the landing legs in the sand. In addition, the penetration provides anchoring to the stage, which prevents toppling motion if there are any environmental disturbances. Priyadarshi et al. reported the earlier studies on the SIS recovery method. The studies concentrated primarily on experimental and finite element analysis of penetration dynamics of the single leg whose velocity is the only variable (two-dimensional analysis), and only limited experimental results are reported for four legs. A systematic effect of the change in impact velocity, attitude, and body rate on the penetration dynamics of the SIS recovery method is not explored.

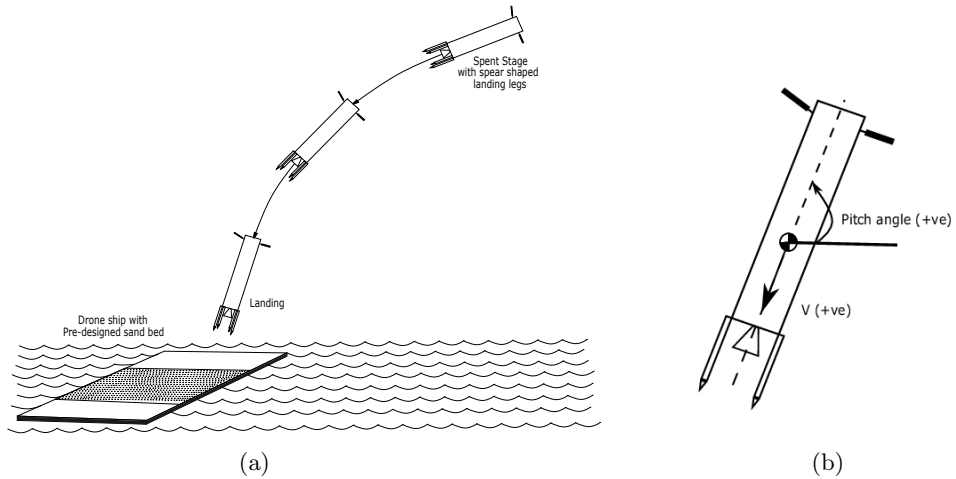


Fig. 1: (a) Schematic of Spear In Sand (SIS) recovery method, and (b) Sign convention

Finding an optimal touchdown state vector that results in minimum impact and guarantees the stability of the stage simultaneously is the first step in the design of spent stage recovery using the SIS method. The problem can be posed as a design optimization problem with the impact force and moment as objective functions. However, because of the absence of deep throttling, some degree of uncertainty is inevitable in the touchdown state vector. The uncertainties may arise from engine shutdown transients, side winds, state tracking errors, and so on. Furthermore, the optimal

touchdown state vector obtained from the deterministic design optimization (DDO) approach may not be reliable and violate the constraints in the presence of uncertainties. Moreover, conventional safety factor-based design approaches could result in a suboptimal design that increases the mass and size of the spent stage. Therefore, the reliability-based design optimization (RBDO) method is attempted in the current study to determine the reliable optimal state vector in the presence of uncertainties. In the RBDO approach, the design variables and (or) parameters are replaced by random variables following a probabilistic distribution, and the objective function is replaced by the expectation of the cost function ($E[f(.)]$), which has to be optimized, satisfying the probabilistic constraints. The probabilistic or reliability constraints are the probabilities of deterministic constraint satisfaction when the design problem is subjected to uncertainties. The major challenge in the RBDO method is the computation of probabilistic constraints (also known as reliability assessment). The reliability assessment has to be performed for each design point traversed by the optimization algorithm. This increases the number of functional evaluations or simulations required for computing the probabilistic estimates for each design point in the optimization loop. Furthermore, it is impractical for cases involving computationally intensive tasks like finite element analysis, computational fluid dynamics, etc. Thus, the RBDO method is often represented in the literature ([Moustapha and Sudret \(2019\)](#); [Dawei et al. \(2021\)](#); [Li et al. \(2021\)](#)) as a two-level approach or nested loop process due to the presence of reliability assessment in the optimization loop.

Many researchers have introduced various indirect methods to overcome the computational complexities. These methods tried to convert the RBDO problem into an equivalent DDO problem and are broadly categorized as double-loop, single-loop, and decoupled methods ([Li et al. \(2021\)](#)). In the double-loop methods, the reliability assessment part is approximated as an equivalent deterministic optimization problem, resulting in an inner optimization loop inside the outer optimization loop. The reliability index approach (RIA) and performance measure approach (PMA) are the most popular double-loop methods. In the RIA method, the probabilistic constraints are converted into deterministic constraints of reliability indices with desired reliable probabilities ([Enevoldsen and Sørensen \(1994\)](#); [Yu et al. \(1997\)](#)). The reliability indices are computed based on the most favourable failure point (or Most Probable Point (MPP), which is found in the inner optimization loop). In the PMA approach, instead of computing the reliability index from the failure point, the algorithm finds the failure point from the desired reliability index (Inverse MPP) in the inner optimization loop ([Youn et al. \(2004\)](#)). Studies have shown that the RIA approach suffers from convergence and stability issues, while PMA is more stable, robust, and yields a higher convergence rate; more importantly, the PMA is computationally less expensive than the RIA ([Tu et al. \(1999\)](#); [Youn and Choi \(2004\)](#)). However, both approaches use approximate methods like the First-Order Reliability Method (FORM) ([Haldar and Mahadevan \(1995\)](#); [Du \(2008\)](#)) and Second-Order Reliability Method (SORM) ([Cizej et al. \(1994\)](#)) for the computation of MPP and IMPP. The FORM and SORM approaches provide accurate solutions for linear and moderately nonlinear problems, and the accuracy degrades with an increase in nonlinearity. Although the PMA is a better approach than RIA, it is still a double-loop method and requires large number of functional evaluations.

The Single-loop methods are introduced to decrease the computational burden of the double-loop methods. [Chen et al. \(1997\)](#) introduced one of the first single-loop approaches, known as the single-loop-single-vector (SLSV) method, for optimizing the weight of a structural member subjected to probabilistic constraints. Later, many researchers used the Karush-Kuhn-Tucker (KKT) optimal conditions to replace the reliability assessment and transform the RBDO to a DDO problem ([Kuschel and Rackwitz \(1997\)](#)). A few researchers proposed hybrid design space approaches by combining the reliability assessment and the objective function ([Kharmanda et al. \(2002\)](#); [Mohsine et al. \(2006\)](#)). The computational efficiency of the single-loop methods is much higher than that of the double-loop methods. However, they suffer from accuracy, convergence, and stability issues for nonlinear problems and are highly dependent on the initial guess ([Aoues and Chateauneuf \(2010\)](#)).

The decoupled methods fill the gaps left by the double-loop and single-loop methods. They isolate the computation of probabilistic constraints from the optimization algorithm and convert the RBDO problem to an equivalent DDO problem. In each iteration, the deterministic constraints get updated (or shifted) towards the design space based on the desired reliable probabilities. In other words, design space is reduced in each iteration to find the optimal solution far away from the actual constraints till the probability of the constraint violation is less than the desired value ([Moustapha and Sudret \(2019\)](#); [Valdebenito and Schüller \(2010\)](#); [Dawei et al. \(2021\)](#)). Decoupled methods gathered much attention from the researchers due to the advantage that reliability assessment is performed only at the deterministic optimal point, which reduces the computational cost drastically without compromising the accuracy. [Weiji and Li \(1994\)](#) investigated the early decoupled methods of linear programming problems by using the reliability index calculated in the preceding iteration. [Du and Chen \(2004\)](#) proposed one of the most popular decoupled methods known as Sequential Optimization and Reliability Assessment (SORA) which updates the constraints by using MPP calculated at the deterministic optimal point. Later, many researchers proposed various variants, viz., enhanced SORA ([Huang et al. \(2012\)](#)), approximate SORA ([Yi et al. \(2016\)](#)), improved SORA ([Choi and Lee \(2018\)](#)), etc. to improve the efficiency of the method. However, the decoupled methods suffer the same disadvantages as single-loop methods due to FORM or SORM approximations and also require a significant number of computationally expensive functional evaluations.

More recently, surrogate models or metamodels have been introduced in optimization problems to reduce the computational cost. The surrogate model (SM) mimics the actual computationally expensive analysis, using known functions and training data (or sampling data), which can be directly employed in the DDO or RBDO problems. The SMs lift the limitation of computationally expensive functional evaluations in the RBDO. Various functions are used as SMs for the RBDO in the literature; these include Kriging functions, Radial Basis Function Neural Networks (RBFNN), Artificial Neural Networks (ANN), Support Vector Machines (SVM), Polynomial Regression, etc. ([Liu et al. \(2018\)](#)). With the help of SMs, the reliability assessment of highly non-linear and non-Gaussian constraints can be done accurately using techniques like Monte Carlo simulations (MCS) rather than FORM or SORM approximations. [Papadrakakis and Lagaros \(2002\)](#) used the MCS with importance sampling for computing the reliability

assessment of a reliability-based structural optimization problem. The authors employed neural networks for approximating probabilistic constraints in first case and approximated the MCS for structural analysis in the second case. [Moustapha and Sudret \(2019\)](#) classified the surrogate-assisted RBDO methods into two branches based on their application. The first branch uses SMs to mimic the reliability assessment part, whereas the second uses them to mimic the objective function and constraints. The second branch is further divided into two sub-branches based on the local and global surrogate modeling. In the first sub-branch, the construction of the SM is embedded in the RBDO algorithm, and the surrogate model is built only in the local regions traversed by the algorithm. This is because, the optimization algorithm traverse only some specific regions in the design space for the solution and the SM is only built in those regions. This method reduces the total number of actual functional evaluations for constructing a SM. [Agarwal and Renaud \(2004\)](#) constructed a response surface near an MPP for the reliability assessment in the double-loop RBDO problem. [Papadrakakis et al. \(2005\)](#) used neural networks for approximating failure probabilities at each iteration in the double-loop optimization process. The major disadvantage with these approaches is that a new surrogate model needs to be constructed in every iteration ([Moustapha and Sudret \(2019\)](#)). Later, [Li et al. \(2019\)](#) proposed sequential SM based de-coupled approach for RBDO in which the SM is constructed only in the neighborhood of optimal point in the previous iteration. The number of total functional evaluations will be less, however, the constructed SM will only serve the optimization purpose and cannot be used for other studies. Moreover, the authors used MCS based reliability assessment to shift the constraints for the next iteration. Although the SM is an analytical function, it requires $10^5 - 10^6$ MCS for accurate estimation of failure probability, since the distributions of probabilistic constraints are unknown. As a result, the computational time increases significantly, especially if the number of constraints are more. Furthermore, the solution can be suboptimal since there is a chance that the algorithm may get stuck at a local minimum.

In the second sub-branch, a global surrogate model is constructed for the entire design space in the first step, and then RBDO is performed ([Dawei et al. \(2021\)](#)). The number of functional evaluations is higher with this approach. However, this can be circumvented using techniques like adaptive sequential (AS) sampling for constructing the training dataset. The AS sampling techniques keep the size of the dataset minimal by choosing the crucial data points sequentially using active learning from previous data points ([Liu et al. \(2018\)](#)). Most of the AS sampling techniques are general for all SMs; however, some AS sampling techniques are more effective against specific SMs. For instance, the gradient-based AS sampling technique is effective for RBFNNs; this is due to the availability of higher-order gradients of RBFNN in analytical form ([Yao et al. \(2009\); Wei et al. \(2012\)](#)), which is also of particular interest in the current study.

In this study, we first present the penetration dynamics of the Spear In Sand (SIS) method using three-dimensional finite element analysis (FEA). Next, we construct a global surrogate model for the FEA using the RBFNNs and second-order gradient-based AS sampling method. The touchdown state vector is the input for the SM, and impact loads and penetration time histories are the output. Furthermore, we formulate

the RBDO problem to find the reliable optimal touchdown state vector with the impact loads as the cost function, which is subjected to the safety probabilistic constraints.

In this article, we extend the second-order gradient-based AS sampling method from single-valued functions to vector-valued functions. Furthermore, we present the Modified Sequential Optimization and Reliability Analysis using the MCS (MSORAMCS) algorithm for solving the RBDO problem. We attempt to reduce the computation time by deducing the parametric distribution of the probabilistic constraints using a statistical test. Once the distribution is known, the parameters can be estimated using fewer MCS. To the best of our knowledge, this is the first work dealing with the in-depth analysis of the SIS recovery approach using the RBDO method. It is also the first attempt to reduce the computation cost of the RBDO algorithm by using a statistic test.

The outline of the current article is as follows, Section 2 explains the three-dimensional finite element analysis and finite element model for the novel SIS recovery method. Section 3 explains the construction of surrogate model for the finite element analysis using the adaptive sequential sampling method. Section 4 introduces the Modified Sequential Optimization and Reliability Assessment using Monte Carlo Sampling (MSORAMCS) RBDO framework for the SIS recovery method. Section 5 shows the validations of proposed methodologies and results obtained using the MSORAMCS algorithm and Section 6 concludes the article.

2 Finite element analysis of SIS recovery method

This section introduces the finite element methodology used for the analysis of the SIS recovery method. Section 2.1 briefs the finite element techniques used for modeling penetration problems, and section 2.2 explains the methodology for modeling the SIS recovery method using the Coupled Eulerian Lagrangian method.

2.1 Finite element analysis

The analysis of the SIS recovery method is very similar to free fall cone penetrometer (FFP) tests in geotechnical engineering, and finite element analysis is extensively used to study the penetration dynamics of FFP tests. The same methodology is used in the current study for the SIS recovery method. The major challenge in the finite element analysis of FFP tests is the heavy mesh distortion due to large deformation, which may lead to early termination of the analysis. Various methods have been introduced to mitigate heavy mesh distortion, like Arbitrary Lagrangian Eulerian (ALE) and Coupled Eulerian-Lagrangian (CEL) methods. The ALE method consists of two parts: creating a new mesh at a given frequency and remapping previous field variables to the new mesh. The field variables are calculated at nodes first (Lagrangian approach), and the new mesh is created by the movement of nodes through the material (Eulerian approach), then the field variables are interpolated to the new mesh nodes ([Hibbit and Sorensen \(2001\)](#); [Carter et al. \(2010\)](#); [Nazem et al. \(2012\)](#)). The method is more suitable for two-dimensional axisymmetric or planar analyses than for three-dimensional analyses due to the huge computation cost. The CEL method combines both Lagrangian and Eulerian approaches in the analysis. In the CEL method,

the body with the higher strength is modeled as a Lagrangian body, and the other body is modeled as an Eulerian body. The difference is that the mesh for Lagrangian bodies is fixed to the material throughout the analysis, whereas for Eulerian bodies, the mesh is fixed in space and the material is allowed to flow inside the mesh. The flow of material inside each element is tracked by a parameter known as the Eulerian Volume Factor (EVF). Since the mesh is fixed in space, there will not be any mesh distortion. Furthermore, it requires less computational cost than the ALE method for three-dimensional analysis. However, due to the Eulerian approach, the stress and strain estimates from the CEL method are less accurate than the ALE method ([Wang et al. \(2015\)](#)). Nevertheless, we focus only on the impact forces and penetration, and therefore the CEL method is adopted for the rest of the study. We reproduced the FFP test cases from [Nazem et al. \(2012\)](#) and validated the CEL approach FFP problems (shown in Figure 2).

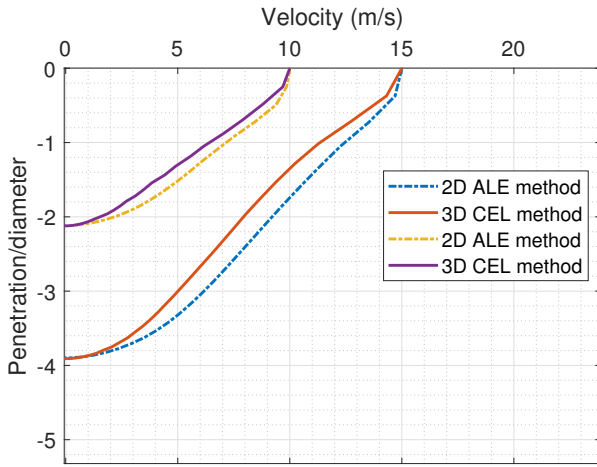


Fig. 2: Validation of CEL method for FFP test cases

2.2 Finite element model

The aim is to carry out a dynamic analysis of the penetration of landing legs in sand using the three-dimensional CEL method. We assume that the thrust is shut down seconds before touchdown and there will be no flow from the nozzle to interact with sand. To reduce the number of independent variables, we limit the attitude and attitude rate only in the pitch direction, which is also the case in the planar conditions. A total of four landing legs are considered for the landing and are modelled as rigid Lagrangian bodies (shown in Figure 3a), and the whole sand domain is modelled as an Eulerian body. Only the four landing legs interact with the sand throughout the analysis; the spent stage above the legs is considered as a point mass residing at the

centre of gravity of the spent stage. Table 1 shows the properties of the spent stage used for the analysis. The dynamic explicit integration scheme is used for the analysis. In geotechnical engineering, the sand or soil behaviour is governed using plasticity models, ranging from the simple Tresca model to advanced hypoplasticity models. In this study, the Drucker-Prager plasticity model, a non-linear sand constitutive model, is chosen for governing the behaviour of the sand. The sand properties used for the analysis are obtained from the various experimental tests conducted at VSSC and are listed in table 2. In the CEL method, the material inside the Eulerian body tries to spill out of the domain while interacting with the Lagrangian body and thus gets excluded from the analysis. A void space needed to be created above the domain without assigning any material to account for the spillage. The sand domain is considered to be a cuboid of size 8 m x 8 m x 8 m, and a void space of 8 m x 8 m x 1 m at the top of the sand domain is configured for eliminating boundary effect and spillage. All surfaces of the sand domain are considered fixed except at the top interface. Figure 3b and 3c show the finite element model and meshed model of the setup, including the void space. A uniform gravity field is applied for the entire setup, and the pitch angle and pitch rate are taken as the attitude and body rate of the spent stage at touchdown. We assumed that the velocity vector is tangential to the axis of the spent stage, and there is no gimbal control of the thrust vector. The touchdown state variables velocity, pitch angle, and pitch rate are given as the input variables to the finite element analysis solver for the dynamic analysis of the penetration process. The analysis is carried out using the ABAQUS Finite Element Analysis solver. The maximum reaction forces (R_x , R_y), reaction moment (R_θ), linear displacement (d_x , d_y), and angular displacement (θ_z) time histories are found out for various combinations of the state variables.

Table 1: Properties of spent stage

Parameter	Value
Mass	8350 kg
Moment of inertia (I_{xx})	$4 \times 10^5 \text{ kgm}^2$
Moment of inertia (I_{yy})	$8 \times 10^3 \text{ kgm}^2$
Moment of inertia (I_{zz})	$4 \times 10^5 \text{ kgm}^2$
Diameter	2.1 m
Geometry of the landing leg	Conical
Apex angle	60°
Diameter of the landing leg	0.15 m

3 Surrogate modelling using adaptive sequential sampling and Radial Basis Function Neural Networks (RBFNN)

With all the known parameters, the finite element analysis can be visualized as a black-box function that takes the input and gives the output. As discussed earlier, the

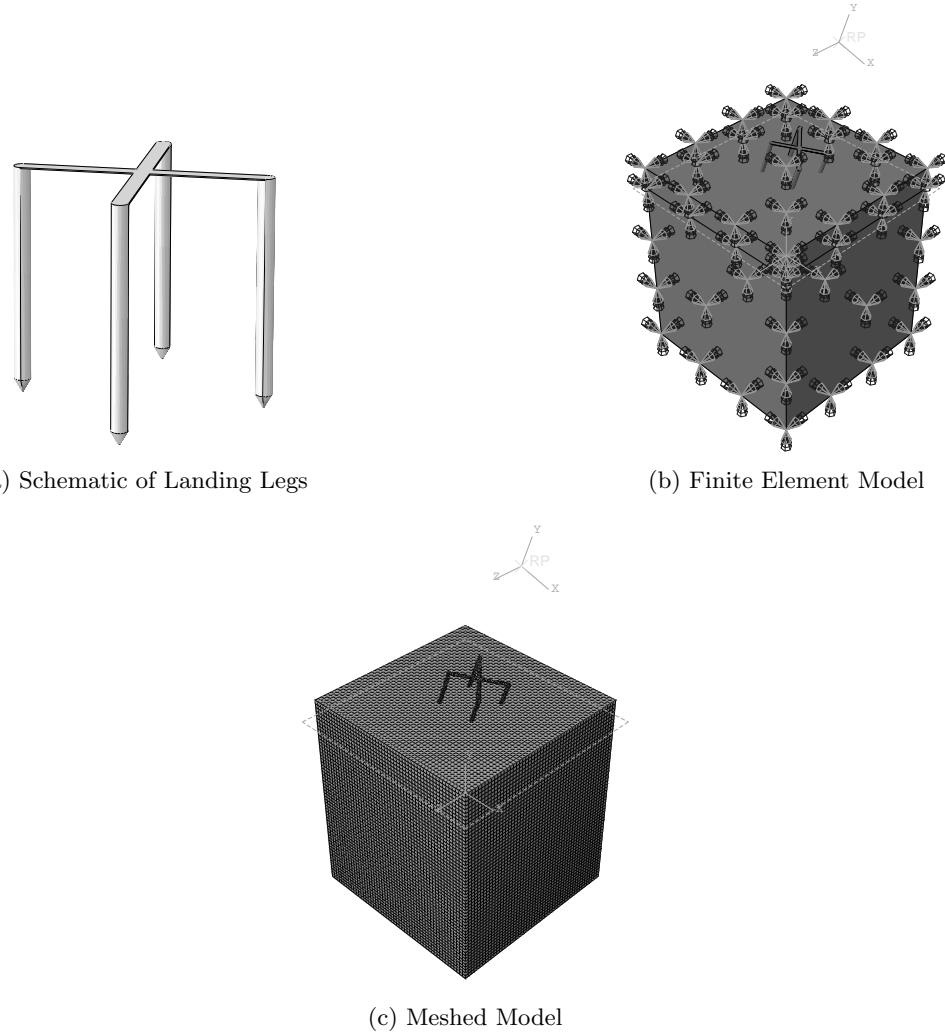


Fig. 3: Finite element model of the SIS recovery method

computationally expensive black-box function cannot be directly used for optimization purposes. The SMs can be helpful in those situations. To make the SM accurately mimic the black box function, it needs to be trained with the actual data from the black box computations. The size of the training data set cannot be too large due to computational limitations, and it cannot be too small, which degrades the accuracy. The training data points must be chosen wisely such that maximum accuracy is obtained with a smaller number of data points. The process of choosing training data points for SMs is known as '*Sampling*'. Many sampling methods have been introduced in recent years that are broadly divided into two categories: one-shot sampling and

Table 2: Properties of the Drucker-Prager model

Parameter	Value
Density (ρ)	1800 kg/m^3
Young's modulus	30 MPa
Poisson's ratio (ν)	0.3
Friction angle (β)	50.57°
Dilation angle (Ψ)	6.08°
Compressive hardening (σ_c)	334.2 kPa
Flow stress ratio (K)	0.778
Frictional coefficient (μ)	0.4

sequential sampling. In the former method, the training data points are chosen in a single step using some rule or an algorithm, whereas, in the latter method, the data points are added to the data set sequentially till it achieves the desired accuracy.

Sequential sampling methods are proven more efficient than one-shot sampling methods because they guarantee the desired accuracy and eliminate unnecessary black box simulations. More research has been focused on sequential sampling methods due to their advantages over other methods, and a new variant known as the Adaptive Sequential (AS) sampling method has been introduced to reduce the number of functional evaluations even more. In AS sampling methods, the sampling algorithm uses previously sampled data to sample new points from the regions that contain crucial information about the black box functions, for instance, the regions that are highly non-linear and are more likely to cause prediction errors. Including the data points from these regions in the training data increases the accuracy of the SM, also decreasing the size of the dataset.

This section presents the surrogate modeling using Radial Basis Function Neural Networks (RBFNN). Section 3.1 introduces the Radial Basis Function Neural Networks (RBFNN) based surrogate modeling and its construction from training data, section 3.2 describes the adaptive sequential sampling method chosen for the current study known as Maximum Curvature Minimum Point Distance based Sequential Sampling (MCMPPDS) method, section 3.3 presents the extension of MCMPPDS method to vector valued functions, and section 3.4 show the construction of the surrogate model for the analysis of the SIS recovery method.

3.1 Radial Basis Function Neural Networks (RBFNN)

The RBFNNs are chosen for the current study due to their simple architecture and ability to interpolate non-linear functions. [Hardy \(1971\)](#) introduced the early RBFNNs to interpolate the uneven topographical contours of geographic data. Unlike other neural networks, RBFNN architecture consists of only one hidden layer with radial basis functions at the neurons, which are used to model the non-linearity of target function. Researchers have introduced many radial basis functions in recent years for different applications; the most commonly used radial basis functions are shown in table 3. The other major advantage of RBFNN is that it requires only one hyperparameter, which can be tuned easily to obtain an accurate surrogate model. For a p-dimensional input

vector, the q-dimensional output vector from the RBFNN can be written as sum of the scalar product of weights and radial basis functions.

$$\hat{y}_j = \sum_{i=1}^N \lambda_{ij} \phi(\|\mathbf{x} - \mathbf{x}_i\|) \quad (1)$$

Where ϕ is the radial basis function, λ_{ij} are the weights, N is the total number of neurons which is equal to the total number of training data points ($[\mathbf{x}_i, \mathbf{y}_i]$), $\|\cdot\|$ denotes the euclidean norm, and j is the component of q-dimensional output vector.

Table 3: Radial Basis Functions

Radial Basis Functions	$\phi(r)^1$
Linear	r
Cubic	$(r+c)^3$
Thin-Plate Spline	$r^2 \ln(cr)$
Gaussian	e^{-cr^2}
Multi-Quadric	$\sqrt{r^2 + c^2}$
Inverse Multi-Quadric	$\frac{1}{\sqrt{r^2 + c^2}}$

¹r is the euclidean norm ($r = \|\mathbf{x} - \mathbf{x}_i\|$)

After creating the training data set of size N and choosing a value for the parameter 'c', the data points can be substituted into equation (1) to form a system of linear equations as follows,

$$\begin{bmatrix} y_{1,1} & \dots & y_{1,q} \\ y_{2,1} & \dots & y_{2,q} \\ \vdots & \ddots & \vdots \\ \vdots & \ddots & \vdots \\ \vdots & \ddots & \vdots \\ y_{N,1} & \dots & y_{N,q} \end{bmatrix} = \begin{bmatrix} \phi(\|\mathbf{x}_1 - \mathbf{x}_1\|) & \dots & \phi(\|\mathbf{x}_1 - \mathbf{x}_N\|) \\ \phi(\|\mathbf{x}_2 - \mathbf{x}_1\|) & \dots & \phi(\|\mathbf{x}_2 - \mathbf{x}_N\|) \\ \vdots & \ddots & \vdots \\ \vdots & \ddots & \vdots \\ \vdots & \ddots & \vdots \\ \phi(\|\mathbf{x}_N - \mathbf{x}_1\|) & \dots & \phi(\|\mathbf{x}_N - \mathbf{x}_N\|) \end{bmatrix} \begin{bmatrix} \lambda_{1,1} & \dots & \lambda_{1,q} \\ \lambda_{2,1} & \dots & \lambda_{2,q} \\ \vdots & \ddots & \vdots \\ \vdots & \ddots & \vdots \\ \vdots & \ddots & \vdots \\ \lambda_{N,1} & \dots & \lambda_{N,q} \end{bmatrix} \quad (2)$$

Now, the weights being only unknowns in the equation (2) can be obtained by inverting the radial basis function matrix and multiplying it with output matrix (shown in equation (3)).

$$\boldsymbol{\lambda}_{N \times q} = \boldsymbol{\Phi}_{N \times N}^{-1} \mathbf{Y}_{N \times q} \quad (3)$$

This completes the training of RBFNN.

3.2 Adaptive Sequential Sampling for RBFNN surrogate model

As discussed earlier, the gradient-based AS sampling methods are best suited for RBFNNs due to the analytical tractability of their higher derivatives. [Liu et al. \(2018\)](#)

proposed a second-order gradient-based method known as the Maximum Curvature Minimum Point Distance Sampling (MCMPDS) method, which uses the second-order gradient information of the surrogate model for sampling new data points. The motivation behind the MCMPDS method is that, graphically, a function value changes drastically near the regions with large curvature; in other words, a high curvature region of a function implies higher non-linearity. These regions are crucial for optimization due to the presence of extremum points, and these are also the regions where the surrogate model is highly likely to make prediction errors. Therefore, the data points from these regions must be included in the training data set for an accurate surrogate model and optimization purposes. The first and second-order gradients for j^{th} component of RBFNN can be written as follows ([Liu et al. \(2018\)](#)),

$$g_j(\mathbf{x}) = \sum_{i=1}^N \frac{\lambda_{ij}\phi'(r_i)}{r_i} (\mathbf{x} - \mathbf{x}_i)^T \quad (4)$$

$$H_j(\mathbf{x}) = \sum_{i=1}^N \frac{\lambda_{ij}}{r_i} \left[\phi'(r_i) \cdot \mathbf{I} + \left(\phi''(r_i) - \frac{\phi'(r_i)}{r_i} \right) \frac{(\mathbf{x} - \mathbf{x}_i)(\mathbf{x} - \mathbf{x}_i)^T}{r_i} \right] \quad (5)$$

where r_i is the euclidean distance between the point \mathbf{x} and i^{th} training data point \mathbf{x}_i .

The MCMPDS method starts with initializing a small data set of input points using any of the one-shot sampling methods, and then the actual outputs from the black box function simulations are computed for these inputs to create a small training data set. In the second step, a preliminary surrogate model is built using the initial training data set. These steps are common for any of the adaptive sequential sampling methods, the fourth step in which the new data point is added to the data set using adaptive sampling criterion makes the difference in most of the methods. The MCMPDS method samples the points by solving an optimization problem which can be formulated as,

$$\begin{aligned} &\text{Maximize } k(\mathbf{x}).d_{min}^D(\mathbf{x}) \\ &\text{W.r.t } \mathbf{x} \\ &\text{Subject to } k(\mathbf{x}) \geq 10^{-8} \end{aligned} \quad (6)$$

Where the first term, $\mathbf{k}(\mathbf{x})$ is the curvature, defined as the square root of the sum of squares of eigen values of the Hessian matrix. The second term, $d_{min}(\mathbf{x})$ is the minimum distance of new point \mathbf{x} from the existing data points and D is the exponent (=2 when the number of input variables is less than or equal to two otherwise 1). The $\mathbf{k}(\mathbf{x})$ in the objective function makes sure that the new point is chosen at large curvature and the $d_{min}(\mathbf{x})$ makes sure that sampling points are widely distributed over the domain and helps avoid sampling from the same area.

The next step is to find the actual output for the newly chosen point from the algorithm, add it to the training data set, and update the RBFNN. The process repeats till it satisfies the stopping criteria. There are various stopping criteria for different adaptive sequential sampling methods. The MCMPDS method follows two stopping criteria: one is the maximum number of black box function simulations (M_1), and the other is the maximum number of continuous *Invalid Sampling Points* (*ISP*) (M_2).

The ISPs are the training data points where adding or removing those points from the training data set does not affect the accuracy of the surrogate model. The continuous ISPs are the subsequent sampling points that meet the following conditions,

$$|y_i - \hat{y}_{i-1}| \leq \delta_a \text{ or } \frac{|y_i - \hat{y}_{i-1}|}{\bar{y}_i} \leq \delta_r \quad (7)$$

Where y_i is the output from the computational model for input \mathbf{x}_i , \hat{y}_{i-1} is the output from RBFNN constructed without the sampling point \mathbf{x}_i , \bar{y}_i is the average of all existing responses, δ_a and δ_r are absolute and relative tolerances. If any of the two stopping criteria is satisfied then the iterations need to be stopped (see [Liu et al. \(2018\)](#) for the detailed algorithm).

There are no universal measures for describing the goodness of the SM. However, there are measures used to assess the accuracy of the SMs by comparing them with a reference. Error-based (MSE, RMSE, etc.) and cross-validation (CV) measures are a few of the most widely used metrics for measuring the accuracy of the SM. The CV error requires only the training data set and is computed by splitting the training data set (outputs and inputs) into 'n' subsets randomly. Then, in each iteration, a subset is taken out, and a surrogate model is fitted to the remaining data points and validated on the chosen data set. The process continues for all subsets, and the sum of the mean square error of all the subsets gives the CV error. In the current study, since obtaining a test data set is extremely difficult, the Leave-One-Out-Cross-Validation (LOOCV) error (CV error when n=1) is chosen as the performance metric.

$$LOOCV = \frac{1}{N} \sum_{i=1}^N [y^{(i)} - \hat{y}^{(i)}]^2 \quad (8)$$

where $y^{(i)}$ is the actual output from the black box simulation, $\hat{y}^{(i)}$ is the output computed using SM without the data point $y^{(i)}$, and N is the size of the training data set.

3.3 Extension to vector-valued functions

[Liu et al. \(2018\)](#) proposed and validated the MCMPDS method for single-valued (one-dimensional output) functions. In this study, we extend the MCMPDS method to vector-valued functions (q-dimensional output) and validate with standard benchmark test cases. For a q-component vector output, there exists a Hessian matrix for each component, and each has its own non-linearity or curvature for an input vector. In the proposed method, the new point is chosen based on the location where at least one component has high non-linearity. We replace the first term in the objective function (equation (6)) with total curvature, which is defined, for a p-dimensional input and q-dimensional output function, as the square root of the total sum of squares of

Eigenvalues of the q hessian matrices, which can be expressed as follows:

$$\mathbf{K}(\mathbf{x}) = \sqrt{\sum_{i=1}^q \sum_{j=1}^p [k_{ij}(\mathbf{x})]^2} \quad (9)$$

where $k_{ij}(\mathbf{x})$ is the j^{th} eigen value of the Hessian matrix corresponding to i^{th} component of the output vector. Similar to this, a family of methods can be synthesized using the eigenvalues of the Hessian matrix. While the proposed method is only a variant, a detailed study of the family of methods will be explored in the future. We validate the proposed approach with the standard vector-valued benchmark functions.

3.3.1 Fonesca Fleming Function

$$f_1(\mathbf{x}) = 1 - e^{\left(-\left[x_1 - \frac{1}{\sqrt{2}}\right]^2 - \left[x_2 - \frac{1}{\sqrt{2}}\right]^2\right)} \quad (10)$$

$$f_2(\mathbf{x}) = 1 - e^{\left(-\left[x_1 + \frac{1}{\sqrt{2}}\right]^2 - \left[x_2 + \frac{1}{\sqrt{2}}\right]^2\right)} \quad (11)$$

$$x_1, x_2 \in [-4, 4] \quad (12)$$

The Fonesca-Fleming function is a 2-dimensional output with a 2-dimensional input function (shown in figures 4a and 4b). A surrogate model is constructed for the Fonesca-Fleming function using RBFNNs and the extended MCMPDS method with an initial dataset of size 25, sampled using grid sampling. For the stopping criteria, we consider the maximum number of functional evaluations (M_1) to be 39, and the number of continuous ISPs to be 3 with a relative tolerance of 0.02. The sampled datapoints obtained using the extended MCMPDS method (shown in figure 4c) fall in the region where at least one component has the highest non-linearity. Furthermore, the Root Mean Square Error (RMSE) (listed in Table. 4) obtained using the extended MCMPDS method is one order of magnitude less than that of the SMs built using standard Grid Sampling (GS) and Latin Hypercube Sampling (LHS) methods.

3.3.2 Viennet Function

$$f_1(\mathbf{x}) = 0.5(x_1^2 + x_2^2) + \sin(x_1^2 + x_2^2) \quad (13)$$

$$f_2(\mathbf{x}) = \frac{(3x_1 - 2x_2 + 4)^2}{8} + \frac{(x_1 - x_2 + 1)^2}{27} + 15 \quad (14)$$

$$f_3(\mathbf{x}) = \frac{1}{x_1^2 + x_2^2 + 1} - 1.1e^{-(x_1^2 + x_2^2)} \quad (15)$$

$$x_1, x_2 \in [-2, 2] \quad (16)$$

Similarly, the extended MCMPDS method is validated against the 3-dimensional output and 2-dimensional input Viennet function (shown in figures 5a, 5b, and 5c). The number of intial data points are same as that of previous case with stopping

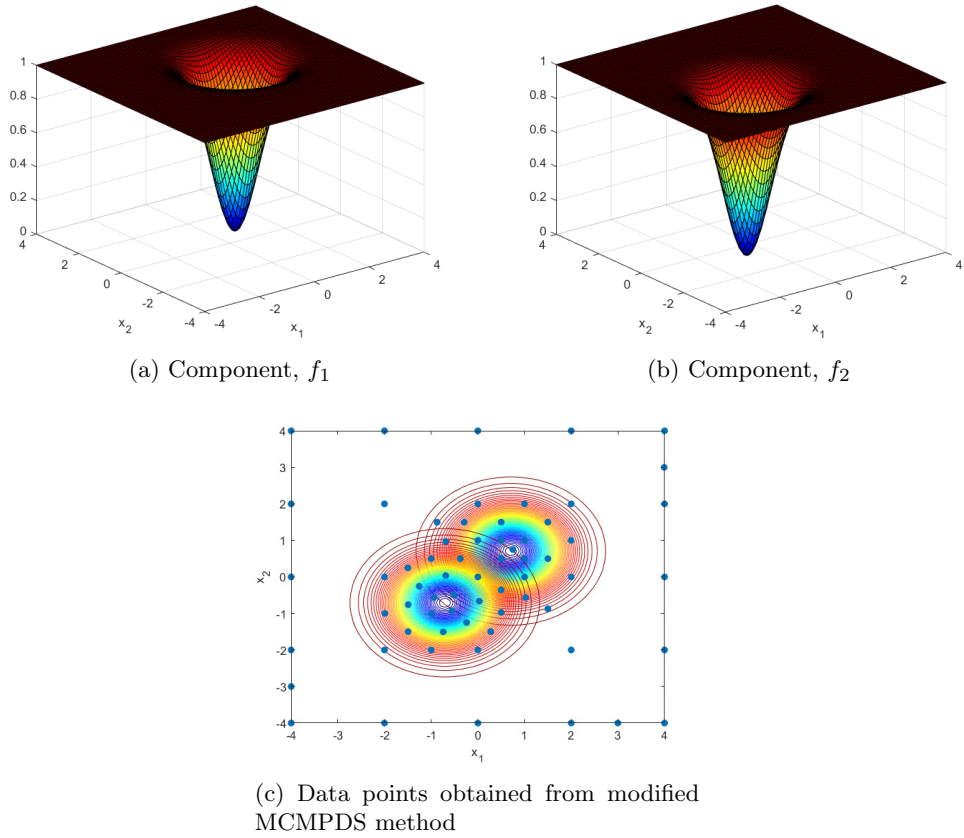


Fig. 4: Validation study of the fonesca-fleming function

Table 4: RMSE of RBFNN for benchmark function using various sampling methods

Sampling method	Fonesca Fleming Function		Viennet Function	
	Number of data points	RMSE	Number of data points	RMSE
Grid sampling	64	0.0225	75	0.0950
Latin hypercube sampling	64	0.0871	75	0.1739
MCMPPDS method	64	0.0088	75	0.0528

criteria $M_1 = 75$, $M_2 = 3$, and $\delta = 0.02$. Figure 5d shows that the sampled points using the extended MCMPPDS method, which are concentrated at the areas with the large curvature (near corners and the centers). Moreover, the RMSE of proposed approach is much lesser than the other sampling methods by nearly a factor of 2. This demonstrates the advantage of sampling near highly non-linear areas (or large curvatures) for better accuracy.

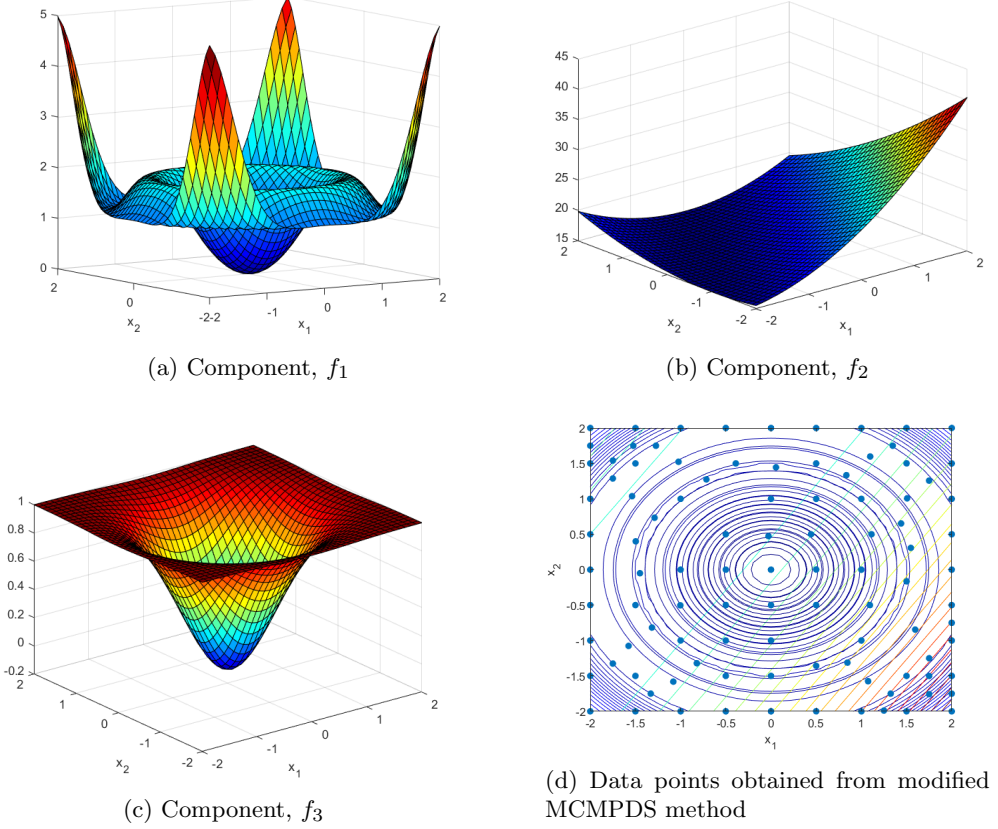


Fig. 5: Validation study of the viennet function

3.4 Surrogate model for SIS recovery method

The required output from the SM is similar to that of finite element analysis, i.e., maximum reaction forces, reaction moment, linear and angular displacement time histories. The maximum reaction forces and moments are discrete values that can be directly given as training data, but the linear and angular displacement time histories are curves and cannot be directly given as training data. Therefore, a cubic polynomial is fitted to the curves and their polynomial coefficients for the given simulation time are taken as the training data. The output dimension for the surrogate model now becomes 15 (two reaction forces, one reaction moment, and twelve polynomial coefficients), while the input is three (touchdown velocity, touchdown pitch angle, and touchdown pitch rate). Figure 6 shows the RBFNN architecture for the current study.

After validation with the benchmark functions, the SM has been constructed for the SIS recovery approach using the extended MCMPDS method. The upper and lower limits of the inputs, velocity, pitch angle, and pitch rate are taken as 0 and 15 m/s, 70° and 90°, -20°/sec and 20°/sec. The size of initial data points is taken as 27 (3^3),

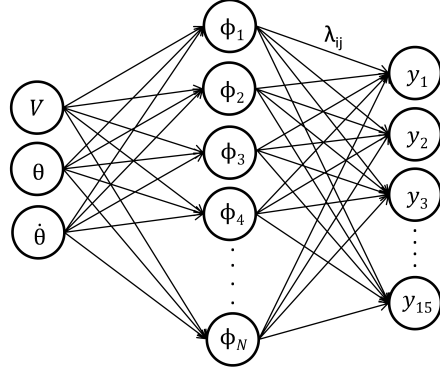


Fig. 6: RBFNN architecture for the analysis of SIS recovery method

which are generated using grid sampling. For stopping criteria, we consider $M_1 = 203$ ($27+203 = 230$ points) and $M_2 = 3$ with a band radius 0.02. We choose the cubic RBF as the activation function for the SM due to the lower error for the SM with the initial population compared to the other activation functions. As said earlier, the LOOCV error is used as the performance indicator for accuracy. However, the order of magnitude of each output component differs considerably due to different types of output; therefore, a normalized leave-one-out cross-validation (NLOOCV) is proposed and employed in the current study, which can be defined as follows:

$$NLOOCV = \frac{1}{N} \sum_{i=1}^N \left(\left\| \frac{y^{(i)}}{\|y^{(i)}\|} - \frac{\hat{y}^{(i)}}{\|y^{(i)}\|} \right\| \right)^2 \quad (17)$$

where $y^{(i)}$ is the actual output, $\hat{y}^{(i)}$ is the output generated using the SM without data point $y^{(i)}$, and N is the total number of data points. Figure 7a shows the variation of the NLOOCV error with the size of the training data. The NLOOCV error decreases with the increase in the size of the data set. However, we can observe the increase in error at few occasions where a new datapoint is added. This is because of large curvature or nonlinearity at those added points, without which there is a high chance of prediction error. Furthermore, it is an indicative of large curvature or non-linearity at the added points.

A validation test case with a velocity of 5 m/s, a pitch angle of 75° , and a pitch rate of $-10^\circ/\text{sec}$ has been done to assess the accuracy of the SM. Figures 7b and 7c show linear and angular displacement obtained using the SM and FEA. The displacement time histories from the SM accurately approximate the actual displacement time histories from the FEA. Table 5 reports the maximum reaction loads and reaction moments obtained using the SM and FEA for the test case, which are very close. The obtained level of accuracy of the SM is sufficient for the current study.

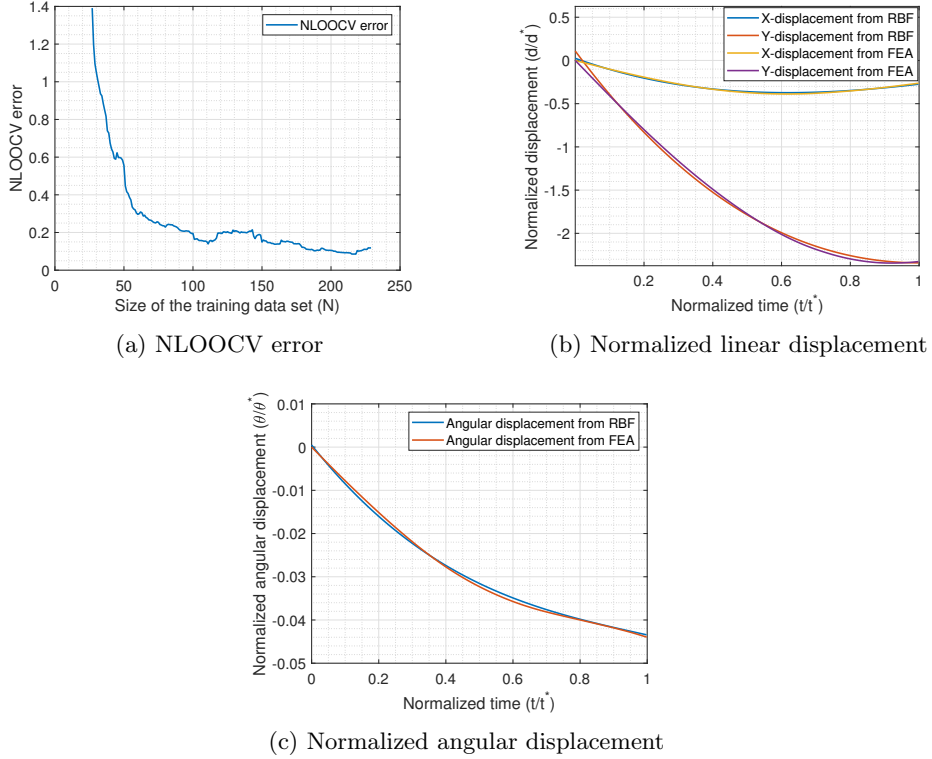


Fig. 7: Validation of the SM for the analysis of SIS recovery method

Table 5: Output from the SM and FEA

Variable	RBFNN with extended MCMPDS method	FEA	% Error
Reaction load in X-direction (R_x/m)	3.05g	2.75g	10.9%
Reaction load in Y-direction (R_y/m)	8.01g	8.19g	2.2%
Reaction moment in pitch direction (R_θ/I)	$2.93^\circ/s^2$	$2.56^\circ/s^2$	14.4%

4 Reliability-Based Design Optimization of SIS recovery method

This section presents the reliability-based design optimization of the SIS recovery method using the modified SORA method. The subsection 4.1 introduces the problem statement; subsection 4.2 briefs the existing methodology of the sequential SORA method using Monte Carlo simulations. Subsection 4.3 presents the modified methodology.

4.1 Problem statement

As discussed earlier, the touchdown state vector is crucial in landing the spent stage successfully. The current study aims to find a touchdown state vector that minimizes the reaction load on the spent stage while ensuring safe landing in the presence of uncertainties. We formulate the problem as follows:

$$\begin{aligned}
 & \text{Minimize} \quad E[J(\mathbf{x} + \boldsymbol{\epsilon})] = \sqrt{R_x^2 + R_y^2 + R_\theta^2} \\
 & \text{s.t.} \quad \begin{aligned}
 c1 : \mathbb{P}[\theta_f(\mathbf{x} + \boldsymbol{\epsilon}) \geq 81.12^\circ] & \geq R_1 \\
 c2 : \mathbb{P}[d_f(\mathbf{x} + \boldsymbol{\epsilon}) \geq 0.3] & \geq R_2 \\
 c3 : \mathbb{P}[d_f(\mathbf{x} + \boldsymbol{\epsilon}) \leq 0.8] & \geq R_3
 \end{aligned} \\
 & \mathbf{x} \in \{\mathbf{x}_L, \mathbf{x}_U\}^T \\
 & \boldsymbol{\epsilon} \sim \mathcal{N}(0, \sigma^2)
 \end{aligned} \tag{18}$$

Here, \mathbf{x} is the expectation of the random variable vector X , which coincides with the touchdown state vector in the current problem; R_x , R_y , and R_θ are the normalized values of maximum reaction loads and moment in the X, Y, and pitch directions during the penetration process. The θ_f and $d_f (= \sqrt{d_X^2 + d_Y^2})$ are the final pitch angle and final depth of penetration after the penetration process respectively. The R_i ($i = 1, 2, 3$) represents the reliability probabilities of the probabilistic constraints, and $\boldsymbol{\epsilon}$ is the uncertainty vector. We assume the uncertainty follows the Gaussian distribution. The probabilistic constraint $\{c1\}$ ensures that the center of gravity of the spent stage will always be inside the projected polygon of the four landing legs with a reliability probability greater than R_1 . It ensures that no adverse moment will be generated, which makes the spent stage fall. The constraint $\{c2\}$ requires that the probability of depth of penetration more than 0.3 m is greater than the reliability probability R_2 . This ensures sufficient anchoring to the spent stage and prevents any toppling motion due to internal and external disturbances after the penetration process. The third constraint $\{c3\}$ requires that the probability of depth of penetration less than 0.8 m is greater than reliability probability R_3 . This is because the length of each landing leg from the nozzle end is considered as 1 m, and this constraint provides sufficient clearance between the sand and the nozzle so that it would not get damaged by the sand. The reliability probability and the standard deviation of the uncertainty are varied to find their effect on the reliable optimum.

4.2 Sequential surrogate model for reliability-based design optimization (SSRBO)

As discussed earlier, [Li et al. \(2019\)](#) proposed the Sequential Surrogate model for the Reliability-Based design Optimization (SSRBO) algorithm using MCS, where construction of the SM is embedded into the algorithm. It starts with building SMs for the objective function and constraints using the initial training dataset. In the second step, an optimization problem, similar to the MCMPDS method, is solved to sample

the new points in the feasible solution space of the problem where the objective function is minimum. The sampling process continues until the termination criterion is achieved and the SM is updated in each iteration. In the third step, deterministic optimization is performed using the SM to find an optimal point, which will be added to the training data set. In the next step, a set of 10^6 points (MCS) are generated using a normal distribution with the optimal point as the expected value with the given standard deviation. Then, the constraint values are evaluated for these points using the SM, and a kernel distribution is fitted to these values using the '*fitdist*' function in MATLAB. The offset by which the constraint must be shifted is obtained using the Inverse Cumulative Distribution Function (ICDF) calculated from constraint distribution and required reliability using the '*icdf*' function in MATLAB. The process continues till it achieves the maximum iteration limit, or the difference between the constraints offsets in the current and previous iterations is less than a given threshold. In each iteration, the actual values of the objective function and the constraints are computed, which will be added to the dataset, and the SM gets updated (refer to [Li et al. \(2019\)](#) for the detailed algorithm).

The advantage of this method is that it provides accurate failure information on the probabilistic constraints since there is no approximation of their distribution. However, fitting kernel distributions to the 10^6 constraint data points is computationally very expensive if the number of constraints is high, which is also the major drawback of this method. Moreover, the obtained SM from the SSRBO algorithm cannot be used for other studies with different objective functions and constraints.

4.3 Modified Sequential Optimization and Reliability Assessment using Monte Carlo simulations (MSORAMCS)

In this study, we attempt to solve the current RBDO problem (equation (18)) using the SSRBO algorithm. Since the SM is readily available, we use only the SORA part of the SSRBO algorithm to solve the present problem.

In general, most of the constraint data obtained from parametric uncertainties follows parametric distributions. However, the distributions are unknown, and assuming a particular distribution might result incorrect solutions. By any means, if we know the parametric distribution a priori of at least one of the constraints data, then 10^3 to 10^4 MCS may be sufficient for estimating the parametric distributions and computing the ICDF to estimate the offset. It substantially lowers the computational cost of the algorithm.

With the above motivation, we present the Modified SORA using the Monte Carlo Simulations (MSORAMCS) algorithm in the current study. In the modified approach, we generate a sample of constraint data points of size n_0 before fitting the kernel distribution step to verify the parametric distribution of the constraints using a statistic test known as '*Anderson-Darling (AD) Test*'. The AD test is similar to the Kolmogorov-Smirnov (KS) test, however, it tests for five parametric distributions (Gaussian, log-normal, exponential, Weibull, and extreme value). The advantage of the AD test is that it gives more importance to the tail part of the CDF than the KS test while testing for the distributions. If the constraints belong to one of the five parametric distributions, then only n_1 MCS are generated, and the parameters are

computed. Typically, $n_1 \geq n_0$ for estimating more accurate parameters of the distributions. If the AD test fails, the algorithm generates n_2 ($n_2 >> n_1$) MCS and proceeds with fitting the non-parametric kernel distribution function. The remaining process is similar to that of the SSRBO algorithm.

The detailed algorithm can be described as follows,

- Step 1: Generate the global SM for the optimization.
- Step 2: Initiate the constraint offset and iterations to zero ($\Delta_0 = \mathbf{0}$, $k = 0$) and define iteration limit k_{max} , required reliability probabilities (R_i), and constraint offset convergence $\|\Delta_k - \Delta_{k+1}\| \leq 0.0001$.
- Step 3: Check for stopping criteria: $k \leq k_{max}$ or $\|\Delta_k - \Delta_{k+1}\| \leq 0.0001$.
- Step 4: Perform the deterministic optimization with the updated constraints.

$$\begin{aligned} \mathbf{x}_k^* &= \underset{\mathbf{x}}{\operatorname{argmin}} J(\mathbf{x}) \\ \text{S.t.,} \\ g_i(\mathbf{x}) + \Delta_{k,i} &\leq 0, \quad i = 1, 2, \dots, N \\ \mathbf{X}_L \leq \mathbf{x} &\leq \mathbf{X}_U \end{aligned}$$

- Step 5: Generate n_0 MCS from normal distribution with \mathbf{x}_k^* as the expected value and the given standard deviation.
- Step 6: Evaluate all the constraint values for the generated MCS and perform AD test for each constraint data.
- Step 7: If any of the constraint data follows parametric distribution, generate n_2 MCS around \mathbf{x}_k^* and fit the parametric distribution for $n_0 + n_1$ samples.
- Step 8: If not, generate n_2 MCS around \mathbf{x}_k^* and fit the kernel distribution.
- Step 9: Compute the ICDF for the parametric and/or non-parametric distributions using the required reliability probabilities.
- Step 10: Update the constraint offset with the computed ICDF.

$$\Delta_{k+1,i} = CDF^{-1}(R_i, \mathbf{x}_k^*) - g_i(\mathbf{x}_k^*), \quad i = 1, 2, \dots, N$$

- Step 11: Go to step 3 and repeat till the termination criterion is achieved. The pseudo code and the flow chart of the proposed algorithm are shown in algorithm 1 and figure 8.

5 RBDO results and discussions

The proposed MSORMCS method is used to solve the SIS problem with $n_0 = 1000$, $n_1 = 5000$, and $n_2 = 10^5$. The algorithm is implemented in MATLAB. We varied the standard deviation of the uncertainty ($\sigma = \{0.01, 0.1, 0.5, 1, 2\}^T \{m/s, deg, deg/s\}$) to find the effect on the reliable optimal solution. To reduce the number of variables, we assumed the reliability probabilities of the constraints to be of the same values. Furthermore, we varied the reliabilities ($R_i = \{0.9, 0.99, 0.995, 0.999\}$) to study the feasibility and its effect on the objective function for higher reliable probabilities. Since uncertainties follow the Gaussian distribution, about 68% of uncertainties fall in the

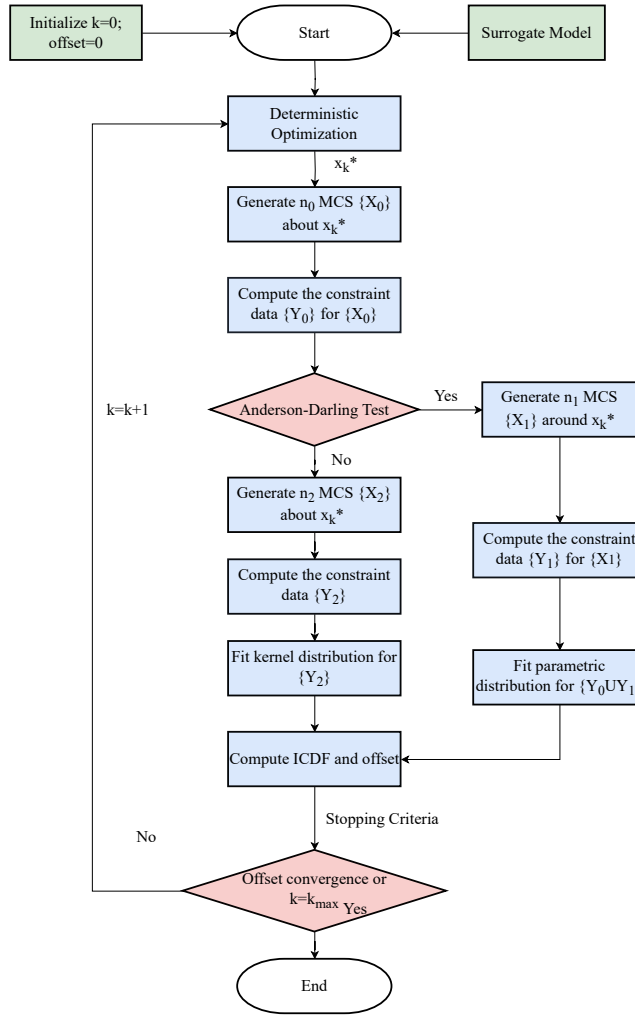


Fig. 8: Flowchart of MSORAMCS method

$\pm\sigma$ region, 95% of uncertainties fall under the $\pm 2\sigma$ region and 99.7% of uncertainties fall in the $\pm 3\sigma$ region. Thus, the design variables are spread over {0.01} to {6} units from the mean, and the reliable optimal solution is obtained by considering these uncertainties.

Figures 9a, 9b, and 9c show the variation of the components of reliable optimal design vector with the variation in the standard deviation of uncertainty and reliability probability. For a given reliable probability, we observe that the reliable optimal touchdown velocity increases linearly with the increase in the standard deviation

Algorithm 1 Modified Sequential Optimization and Reliability Assessment using Monte Carlo simulation (MSORAMCS)

```

1: Input: Maximum iterations ( $k_{max}$ ), reliability probabilities ( $R_i$ ), offset convergence threshold  $\|\Delta_k - \Delta_{k+1}\| \leq 0.0001$ , standard deviation of the uncertainty ( $\sigma$ ), upper and lower limits of design vector  $\{\mathbf{X}_L, \mathbf{X}_U\}$ , probabilistic constraints  $\{c\}$ , size of MCS  $\{n_0, n_1, n_2\}$ 
2: Output: Reliable optimum  $\{\mathbf{x}^*\}$ .
3: Initialize  $k = 0$ ;  $\Delta_0 = \{0, 0, 0, \dots, 0\}^T$ .
4: while  $k \leq k_{max}$  or  $\|\Delta_k - \Delta_{k+1}\| \leq 0.0001$  do
5:    $\mathbf{x}_k^* = \operatorname{argmin}_x J(\mathbf{x})$  s.t.,  $g_i(\mathbf{x}) + \Delta_{k,i} \leq 0$ ,  $i = 1, 2, \dots, N$ 
6:   Generate MCS set  $\{\mathbf{X}_0\}$  with size  $n_0$  following  $\mathbf{X}_0 \sim \mathcal{N}(\mathbf{x}_k^*, \sigma^2)$ 
7:   Compute the constraint data  $\{\mathbf{Y}_0\}$  for  $\{\mathbf{X}_0\}$ .
8:   for  $i=1$  to  $N$  do
9:     if 'adtest' is true then
10:       Generate MCS set  $\{\mathbf{X}_1\}$  with size  $n_1$  following  $\mathbf{X}_1 \sim \mathcal{N}(\mathbf{x}_k^*, \sigma^2)$ 
11:       Compute constraint data  $\{\mathbf{Y}_1\}$  for the set  $\{\mathbf{X}_1\}$ .
12:       Fit the parametric distribution for the data  $\{\mathbf{Y}_0 \cup \mathbf{Y}_1\}$ .
13:     else
14:       Generate MCS set  $\{\mathbf{X}_2\}$  with size  $n_2$  following  $\mathbf{X}_2 \sim \mathcal{N}(\mathbf{x}_k^*, \sigma^2)$ 
15:       Compute constraint data  $\{\mathbf{Y}_2\}$  for the set  $\mathbf{X}_2$ .
16:       Fit the kernel distribution for  $\{\mathbf{Y}_2\}$ .
17:     end if
18:     Compute and update the constraint offset
19:      $\Delta_{k+1,i} = CDF^{-1}(R_i, \mathbf{x}_k^*) - g_i(\mathbf{x}_k^*)$ ,  $i = 1, 2, \dots, N$ 
20:   end for
21:    $k \Leftarrow k + 1$ 
22: end while

```

of the uncertainty. Furthermore, the slope of the velocity versus standard deviation of the uncertainty curve increases with an increase in the reliability probability, as expected. It is because the uncertainties vary from $\pm\sigma$ to $\pm3\sigma$, and the RBDO algorithm must find a solution compatible with these dispersions to achieve the given reliability probability. The higher touchdown velocities guarantee that the minimum depth of penetration constraint is satisfied.

The same trend applies to the reliable optimal pitch angle. Further, the pitch angle is non-vertical for the smaller standard deviation (close to the deterministic optimum). This is because the non-vertical pitch angle distributes the impact load in the vertical and horizontal directions. Moreover, as the standard deviation of the uncertainty and reliability probability increases, the reliable optimal pitch angle moves towards 90° . This is due to the pitch angle constraint, and the vertical attitude ensures that the final pitch angle constraint is satisfied for the given reliability probability and uncertainties.

The variation of reliable optimal pitch rates seems to be negative and non-linear with the standard deviation of uncertainty and reliability probability (see figure 1b for sign convention). The negative pitch rate attempts to make the spent stage inclined

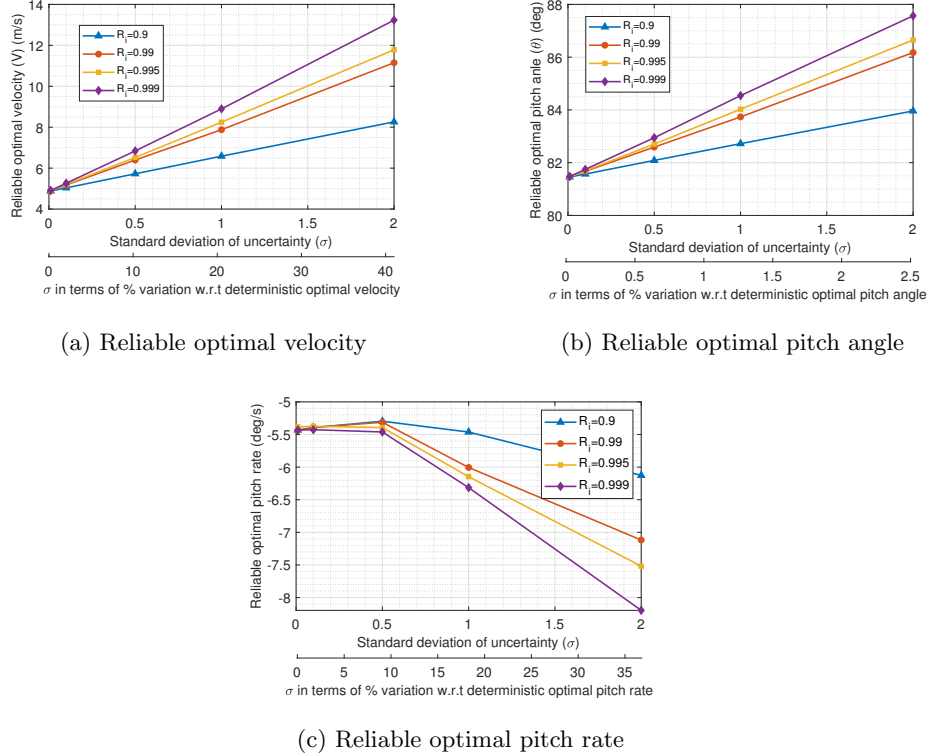
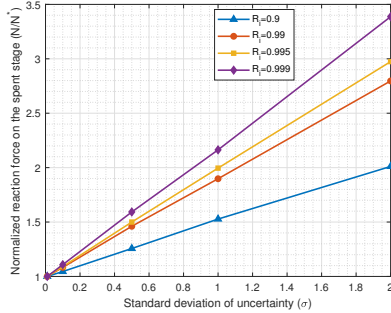


Fig. 9: Variation of reliable optimal solution with reliable probabilities and standard deviation of uncertainty

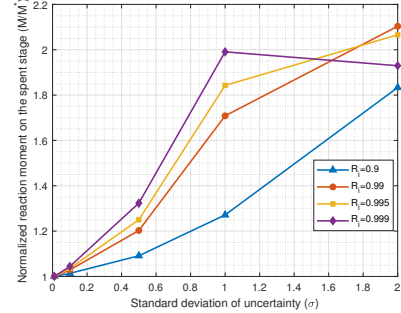
(or non-vertical pitch angle), which results in less impact. For a smaller standard deviation, the pitch rates are almost the same. This is because the penetration process is almost instantaneous, and the effect of pitch rate is minimal compared to the pitch angle. However, the magnitude increases with an increase in the standard deviation and the reliability probability. This is because, as the pitch angle becomes more vertical with the increase in standard deviation and reliability probability, the pitch rate increases to make the spent stage inclined.

Figures 10a and 10b show the normalized loads corresponding to the reliable optimal solutions. The resultant reaction force follows the same trend as the optimal velocity and pitch angle. It is due to the increase in touchdown velocity and near-vertical pitch angle, which increases the reaction force on the spent stage. However, the variation of the reaction moment is non-linear with the reliability probabilities. This is because when the optimal pitch angle becomes nearly vertical and the touchdown velocity increases, the reaction force on the spent stage becomes more dominant.

We validated the performance of the proposed MSORAMCS approach on the current problem by removing the statistical test part from the algorithm. Now, the

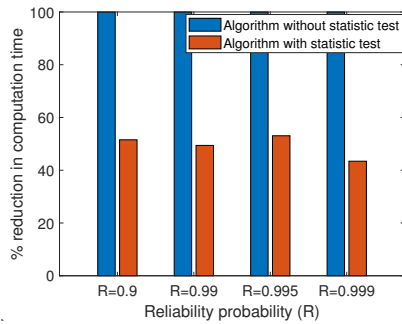


(a) Normalized reaction loads

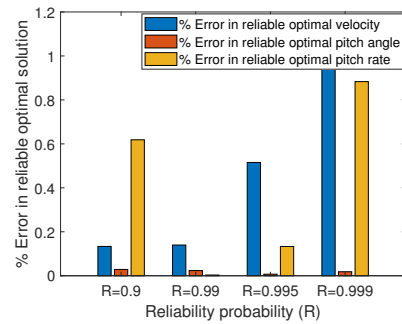


(b) Normalized reaction moments

Fig. 10: Variation of reaction loads with reliable probabilities and standard deviation of uncertainty



(a) Percentage reduction in computation time



(b) Percentage error in optimal solution

Fig. 11: Performance evaluation of the proposed MSORAMCS method

algorithm generates 10^5 MCS for every constraint after the deterministic optimization step and fits the kernel distribution to the data. Figures 11a and 11b show the percentage reduction in the computation time and the accuracy of the obtained solutions for a case with $\sigma = 0.5$ and $R_i = \{0.9, 0.99, 0.995, 0.999\}$. We observe that there is an average reduction of 49.36% in computation time using the statistic test (AD test) after the deterministic optimization step. Furthermore, the percentage error in the reliable optimal solutions obtained with and without using the AD test is less than 1%. It is evident that the proposed method with the modification significantly reduced the computation time without compromising the accuracy of the solution.

6 Conclusions

The current study presents a novel VTVL spent stage recovery approach known as the Spear In Sand (SIS) method. The approach does not require deep throttling of the

engine to achieve zero body rates and velocity at touchdown. Furthermore, the study aims to find an optimal touchdown state vector that results in the safe landing of the spent stage in the presence of uncertainties.

The major contributions of the present paper can be listed as follows,

1. The landing dynamics of the SIS recovery method are formulated using the finite element analysis.
2. A surrogate model is constructed for the finite element analysis using the Radial Basis Function Neural Networks and second-order gradient-based adaptive sequential sampling approach.
3. The adaptive sequential sampling approach is extended and validated for the vector-valued functions.
4. The problem of obtaining a reliable optimal touchdown state vector is formulated as a reliability-based design optimization problem with the impact loads as the cost function.
5. A Monte Carlo-based sequential optimization and reliability assessment framework is chosen for the current study to solve the SIS landing problem.
6. Furthermore, we modified the algorithm by adding a statistic test known as the Anderson-Darling test for obtaining the apriori information of the constraint data distribution.
7. The modified framework yielded nearly 50% reduction in computation time with less than 1% error in the reliable optimal solution for the current problem.

The existence of the reliable optimal solution for higher reliable probabilities ($R_i = 0.999$) provides confidence for the safe landing of the spent stage using the SIS recovery approach. Furthermore, the modified framework can be augmented with other Monte Carlo-based approaches for RBDO problems. Nevertheless, the robustness of the proposed framework has to be verified for non-parametric uncertainties. The future work focuses on finding the optimal policy for the guidance and control of the SIS method from the atmospheric phases, based on the obtained optimal touchdown state vector by formulating a Stochastic Non-linear Optimal Control (SNOC) problem.

Declarations

Author contribution. Deva Karthik Lakshman Dasu: worked on MCMPDS and MSORAMCS algorithms, FEA, code, and drafted the manuscript. Pankaj Priyadarshi: critically reviewed and enhanced the modified algorithms, proposed and performed initial studies of the SIS recovery method, and approved the final manuscript.

Funding. The current study is supported by Vikram Sarabhai Space Center (VSSC), ISRO.

Conflict of interest. The authors declare no competing interests.

...

References

- Agarwal H, Renaud J (2004) Reliability based design optimization using response surfaces in application to multidisciplinary systems. *Engineering Optimization* 36(3):291–311. <https://doi.org/10.1080/03052150410001666578>
- Aoues Y, Chateauneuf A (2010) Benchmark study of numerical methods for reliability-based design optimization. *Structural and Multidisciplinary Optimization* 41(2):277–294. <https://doi.org/10.1007/s00158-009-0412-2>
- Carter JP, Nazem M, Airey DW, et al. (2010) Dynamic Analysis of Free-Falling Penetrometers in Soil Deposits, pp 53–68. [https://doi.org/10.1061/41095\(365\)3](https://doi.org/10.1061/41095(365)3)
- Casiano MJ, Hulka JR, Yang V (2010) Liquid-propellant rocket engine throttling: A comprehensive review. *Journal of Propulsion and Power* 26(5):897–923. <https://doi.org/10.2514/1.49791>
- Chen X, Hasselman T, Neill D (1997) Reliability based structural design optimization for practical applications. In: 38th Structures, Structural Dynamics, and Materials Conference. AIAA, Florida
- Choi SH, Lee I (2018) Improved sequential optimization and reliability assessment for reliability-based design optimization. In: Schumacher A, Vietor T, Fiebig S, et al. (eds) *Advances in Structural and Multidisciplinary Optimization*. Springer International Publishing, Cham, pp 289–298
- Cizelj L, Mavko B, Riesch-Oppermann H (1994) Application of first and second order reliability methods in the safety assessment of cracked steam generator tubing. *Nuclear Engineering and Design* 147(3):359–368. [https://doi.org/10.1016/0029-5493\(94\)90218-6](https://doi.org/10.1016/0029-5493(94)90218-6)
- Dawei Z, Jinyu Z, Chunqiu L, et al. (2021) A short review of reliability-based design optimization. *IOP Conference Series: Materials Science and Engineering* 1043(3):032041. <https://doi.org/10.1088/1757-899X/1043/3/032041>
- Du X (2008) Unified Uncertainty Analysis by the First Order Reliability Method. *Journal of Mechanical Design* 130(9):091401. <https://doi.org/10.1115/1.2943295>
- Du X, Chen W (2004) Sequential Optimization and Reliability Assessment Method for Efficient Probabilistic Design . *Journal of Mechanical Design* 126(2):225–233. <https://doi.org/10.1115/1.1649968>
- Enevoldsen I, Sørensen J (1994) Reliability-based optimization in structural engineering. *Structural Safety* 15(3):169–196. [https://doi.org/10.1016/0167-4730\(94\)90039-6](https://doi.org/10.1016/0167-4730(94)90039-6)

- Haldar A, Mahadevan S (1995) First-Order and Second-Order Reliability Methods, Springer US, Boston, MA, pp 27–52. https://doi.org/10.1007/978-1-4615-1771-9_3
- Hardy RL (1971) Multiquadric equations of topography and other irregular surfaces. Journal of Geophysical Research (1896-1977) 76(8):1905–1915. <https://doi.org/10.1029/JB076i008p01905>
- Hibbit K, Sorensen (2001) ABAQUS/Explicit : user's manual, version 6.2 edn. Hibbit, Karlsson and Sorenson Inc., [Pawtucket, R.I.]
- Huang HZ, Zhang X, Liu Y, et al. (2012) Enhanced sequential optimization and reliability assessment for reliability-based design optimization. Journal of Mechanical Science and Technology 26(7):2039–2043. <https://doi.org/10.1007/s12206-012-0511-7>
- Kharmanda G, Mohamed A, Lemaire M (2002) Efficient reliability-based design optimization using a hybrid space with application to finite element analysis. Structural and Multidisciplinary Optimization 24(3):233–245. <https://doi.org/10.1007/s00158-002-0233-z>
- Kuschel N, Rackwitz R (1997) Two basic problems in reliability-based structural optimization. Mathematical Methods of Operations Research 46(3):309–333. <https://doi.org/10.1007/BF01194859>
- Li X, Gong C, Gu L, et al. (2019) A reliability-based optimization method using sequential surrogate model and monte carlo simulation. Structural and Multidisciplinary Optimization 59(2):439–460. <https://doi.org/10.1007/s00158-018-2075-3>
- Li X, Yang Q, Wang Y, et al. (2021) Development of surrogate models in reliability-based design optimization: A review. Mathematical Biosciences and Engineering 18(5):6386–6409. <https://doi.org/10.3934/mbe.2021317>
- Liu H, Ong YS, Cai J (2018) A survey of adaptive sampling for global metamodeling in support of simulation-based complex engineering design. Structural and Multidisciplinary Optimization 57(1):393–416. <https://doi.org/10.1007/s00158-017-1739-8>
- Mohsine A, Kharmanda G, El-Hami A (2006) Improved hybrid method as a robust tool for reliability-based design optimization. Structural and Multidisciplinary Optimization 32(3):203–213. <https://doi.org/10.1007/s00158-006-0013-2>
- Moustapha M, Sudret B (2019) Surrogate-assisted reliability-based design optimization: a survey and a unified modular framework. Structural and Multidisciplinary Optimization 60(5):2157–2176. <https://doi.org/10.1007/s00158-019-02290-y>
- Nazem M, Carter J, Airey D, et al. (2012) Dynamic analysis of a smooth penetrometer free-falling into uniform clay. Géotechnique 62(10):893–905. <https://doi.org/10.1680/geot.10.P.055>

- Papadrakakis M, Lagaros ND (2002) Reliability-based structural optimization using neural networks and monte carlo simulation. Computer Methods in Applied Mechanics and Engineering 191(32):3491–3507. [https://doi.org/10.1016/S0045-7825\(02\)00287-6](https://doi.org/10.1016/S0045-7825(02)00287-6)
- Papadrakakis M, Lagaros N, Plevris V (2005) Design optimization of steel structures considering uncertainties. Engineering Structures 27(9):1408–1418. <https://doi.org/10.1016/j.engstruct.2005.04.002>
- SpaceX (2025) Falcon 9. <https://www.spacex.com/vehicles/falcon-9/>, accessed: 21-06-2025
- Tu J, Choi KK, Park YH (1999) A New Study on Reliability-Based Design Optimization. Journal of Mechanical Design 121(4):557–564. <https://doi.org/10.1115/1.2829499>
- Valdebenito MA, Schuëller GI (2010) A survey on approaches for reliability-based optimization. Structural and Multidisciplinary Optimization 42(5):645–663. <https://doi.org/10.1007/s00158-010-0518-6>
- Wang D, Bienen B, Nazem M, et al. (2015) Large deformation finite element analyses in geotechnical engineering. Computers and Geotechnics 65:104–114. <https://doi.org/10.1016/j.compgeo.2014.12.005>
- Wei X, Wu YZ, Chen LP (2012) A new sequential optimal sampling method for radial basis functions. Applied Mathematics and Computation 218(19):9635–9646. <https://doi.org/10.1016/j.amc.2012.02.067>
- Weiji L, Li Y (1994) An effective optimization procedure based on structural reliability. Computers & Structures 52(5):1061–1067. [https://doi.org/10.1016/0045-7949\(94\)90090-6](https://doi.org/10.1016/0045-7949(94)90090-6)
- Yao W, Chen X, Luo W (2009) A gradient-based sequential radial basis function neural network modeling method. Neural Computing and Applications 18(5):477–484. <https://doi.org/10.1007/s00521-009-0249-z>
- Yi P, Zhu Z, Gong J (2016) An approximate sequential optimization and reliability assessment method for reliability-based design optimization. Structural and Multidisciplinary Optimization 54(6):1367–1378. <https://doi.org/10.1007/s00158-016-1478-2>
- Youn BD, Choi KK (2004) A new response surface methodology for reliability-based design optimization. Computers & Structures 82(2):241–256. <https://doi.org/10.1016/j.compstruc.2003.09.002>
- Youn BD, Choi KK, Yang RJ, et al. (2004) Reliability-based design optimization for crashworthiness of vehicle side impact. Structural and Multidisciplinary

Optimization 26(3):272–283. <https://doi.org/10.1007/s00158-003-0345-0>

Yu X, Choi KK, Chang KH (1997) A mixed design approach for probabilistic structural durability. Structural optimization 14(2):81–90. <https://doi.org/10.1007/BF01812509>